AGU PUBLICATIONS

Geophysical Research Letters

RESEARCH LETTER

10.1002/2015GL063501

Key Points:

- Felsic interpretations are not consistent with TIR data
- Low abundances of mafics are not required to detect feldspar in the NIR
- Feldspar-enriched eruptive products can be produced from known Martian basalts

Supporting Information:

- Texts S1 and S2, Figures S1 and S2, and Table S1

Correspondence to:
A. D. Rogers,
Deanne.Rogers@stonybrook.edu

Citation:
Rogers, A. D., and H. Nekvasil (2015), Feldspathic rocks on Mars: Compositional constraints from infrared spectroscopy and possible formation mechanisms, *Geophys. Res. Lett.*, *42*, doi:10.1002/2015GL063501.

Received 13 FEB 2015
Accepted 29 MAR 2015
Accepted article online 2 APR 2015

Feldspathic rocks on Mars: Compositional constraints from infrared spectroscopy and possible formation mechanisms

A. Deanne Rogers[1] and Hanna Nekvasil[1]

[1]Department of Geosciences, State University of New York at Stony Brook, Stony Brook, New York, USA

Abstract Rare feldspar-dominated surfaces on Mars were previously reported based on near-infrared (NIR) spectral data and were interpreted to consist of anorthosite or felsic rocks. Using thermal infrared (TIR) data over the feldspar detections with the largest areal extent in Nili Patera and Noachis Terra, we rule out felsic interpretations. Basaltic or anorthositic compositions are consistent with TIR measurements, but the geologic contexts for these regions do not support a plutonic origin. Laboratory NIR spectral measurements demonstrate that large plagioclase crystals ($>\sim 840\ \mu m$) can be detected in mixtures with as much as 50 vol % mafics, which is higher than the previously stated requirement of no more than 15% mafics. Thus, anorthositic or felsic interpretations need not be invoked for all NIR-based feldspar detections. Plagioclase-enriched basaltic eruptive products can be formed from Martian basalts through partial crystallization at the base of a thick crust, followed by low-pressure crystallization of the residual liquids.

1. Introduction

Feldspar-dominated lithologies were previously identified in restricted locations on Mars using high-resolution near-infrared (NIR) imaging spectrometer data from the Mars Reconnaissance Orbiter Compact Reconnaissance Imaging Spectrometer for Mars (CRISM) and the Mars Express Observatoire pour la Minéralogie, l'Eau, les Glaces et l'Activité [*Carter and Poulet*, 2013; *Wray et al.*, 2013]. Detection of feldspar in the near-infrared (NIR) is based on the presence of a broad reflectance minimum between ~1.2 and 1.3 μm that arises from trace amounts of Fe^{2+} substituting for Ca in plagioclase [e.g., *Adams and Goullaud*, 1978]. Previous laboratory studies on controlled mineral mixtures have shown that this band is only detectable when $<$15% mafic minerals or opaques are present in the mixture [*Nash and Conel*, 1974; *Crown and Pieters*, 1987]. The requirement for such a low abundance of mafic minerals has led to two different lithologic interpretations: that these rocks are anorthosites [*Carter and Poulet*, 2013], which contain $>$90% plagioclase, and/or felsic rocks [*Wray et al.*, 2013], which contain not only plagioclase and commonly alkali feldspar but also significant abundances of quartz and/or rhyolitic glass. These lithologies are distinct mineralogically and chemically, and imply very different petrologic histories. Anorthositic lithologies, based on terrestrial and lunar analogs, form through flotation during magmatic differentiation of either a magma ocean or large pluton [e.g., *Emslie*, 1978; *Longhi*, 2003]. Felsic rocks not associated with plate margin tectonics on Earth form as late-stage differentiates of a basaltic parent (for example, Thingmuli Volcano, Iceland [e.g., *Carmichael*, 1964]) or possibly as partial melts of the crust [e.g., *Chappell et al.*, 2004]. A key chemical difference is the silica content, with the bulk composition of anorthosites containing typically ~52 wt % SiO_2, whereas felsic rocks contain $>$ 65% SiO_2 [e.g., *LeMaitre* 1976; *Lindsley et al.*, 2010]. Hereafter, both of these lithologic types are collectively referred to as "feldspathic," a term inclusive of both lithologies.

The detections of feldspathic units occur in a variety of contexts, including the walls of craters and valleys [*Carter and Poulet*, 2013], crater central peaks, the intercrater plains and intracrater floors of Noachis Terra, and the caldera floor of Nili Patera [*Wray et al.*, 2013]. Most of the detections are areally minor ($<$1 km^2), with some larger detections spanning ~10^0–10^1 km, located in Nili Patera and Noachis Terra. In addition, many of the detections are colocated with phyllosilicate minerals. The compositional and geologic characteristics of terrains in the vicinity of the Nili Patera and Noachis Terra NIR feldspar detections were described in previous studies [*Christensen et al.*, 2005; *Rogers et al.*, 2009; *Skok et al.*, 2010; *Rogers and Nazarian*, 2013]; the findings from those studies are summarized below.

In Nili Patera, the locations of feldspathic rock detections reported by *Wray et al*. [2013] are contained within a bedrock unit that was previously mapped as olivine basaltic by *Christensen et al*. [2005] using thermal infrared data from the Mars Odyssey Thermal Emission Imaging System (THEMIS) and the Mars Global Surveyor Thermal Emission Spectrometer (TES). The olivine basaltic unit is overlain by basaltic dunes in the southern portion of the caldera, as well as by a volcanic construct and flow in the northeastern portion of the caldera. The THEMIS and TES data over the volcanic construct and flow are consistent with high abundances of felsic glass, suggesting a bulk composition with intermediate-silica content, termed "dacitic" by *Christensen et al*. [2005]. Importantly, the term "dacite" has been used for rocks with such silica contents on Mars, but its use does not imply any association with subduction zone magmas, in spite of such rocks on Earth being found only in such regimes. Later analyses by *Skok et al.* [2010] using CRISM data showed the presence of hydrated silica associated with portions of the dacitic lava flow unit reported by *Christensen et al*. [2005].

In Noachis Terra, feldspathic detections reported by *Wray et al*. [2013] correspond to "light-toned" units mapped by *Rogers and Nazarian* [2013] (and were originally designated "red" units by *Rogers et al*. [2009], based on the color of their appearance in false-color THEMIS images). These units, which span tens of kilometers in many cases, exhibit high thermal inertias and deep spectral contrast, consistent with competent, nonporous rock. *Rogers and Nazarian* [2013] reported that the light-toned units commonly overlie olivine basaltic bedrock and are ~20–25 m thick. Locations where the stratigraphic contact between these units is present are found in many isolated locations separated by hundreds of kilometers. The olivine basaltic bedrock units fill topographic lows, exhibit embayment relationships with preexisting terrain, and are compositionally distinct, suggesting a volcanic (effusive) origin. Because the light-toned units are typically found overlying the olivine basaltic units, *Rogers and Nazarian* [2013] assumed a genetic relationship between the two units and suggested that they could represent successive members of a flood basalt sequence, with slight differences in feldspar/pyroxene ratio. It is possible, however, that the two units were commonly preserved, rather than commonly emplaced.

Here we provide additional constraints on the nature of these feldspathic detections using a combination of geologic context observations, orbital thermal infrared measurements, and laboratory near-infrared spectral measurements of coarse-grained mineral mixtures. We show that felsic lithologies can be ruled out for all detections that are spatially resolved by THEMIS. Anorthosites are consistent with THEMIS data and for most of the geologic contexts; however, for some geologic contexts, anorthosites are unlikely. Thus, for those cases, we examine alternative spectral analogs, as well as alternative mechanisms for forming feldspar-rich lavas.

2. Constraints From Thermal Infrared and Near-Infrared Spectroscopy

Thermal infrared spectroscopy is sensitive to SiO_2 content [e.g., *Lyon*, 1965]. Figure 1a shows laboratory thermal emission spectra of felsic rocks and anorthosite; basaltic/mafic and ultramafic rocks are shown for comparison. These three classes of rocks are easily distinguished from one another at laboratory spectral resolution, with major differences in the center position of the Si-O-related molecular vibrational absorptions between ~8 and 12 μm, and significant differences in the overall spectral shape at longer wavelengths ~20–50 μm. Figure 1b shows how these spectra appear when degraded to the resolution and sampling of THEMIS [*Christensen et al*., 2004], which acquires multispectral thermal infrared (TIR) images of Mars at a spatial resolution of 100 m/pixel. At THEMIS spectral resolution, anorthosites remain spectrally distinct from felsic rocks; however, distinguishing anorthosites from mafic rocks becomes challenging.

We utilize the position of the broad emissivity minimum between ~8 and 12 μm (Figure 1) to locate possible felsic surface compositions in atmospherically corrected [*Bandfield et al*., 2004] THEMIS data. To estimate the wavelength position of the surface emissivity minimum, we calculate a cubic spline interpolation [e.g., *Ueberhuber*, 1997] to atmospherically corrected THEMIS emissivity spectra (bands 3–9). The wavelength position of the spline fit minimum (SFM) is then mapped on a pixel-by-pixel basis. Similar techniques to parameterize the shape and/or minimum of emissivity spectra have been successfully applied to THEMIS data as well as terrestrial thermal infrared multispectral data in previous studies [*Hook et al*., 2005; *Smith et al*., 2013; *Pan et al*., 2015]. Figure 1b shows example cubic spline fits to laboratory thermal emission spectra (degraded using THEMIS filter response functions) from felsic, anorthositic, mafic, and ultramafic rocks. The SFM values for these rocks are given in the spectrum labels, in parentheses (Figure 1b). Additional SFM

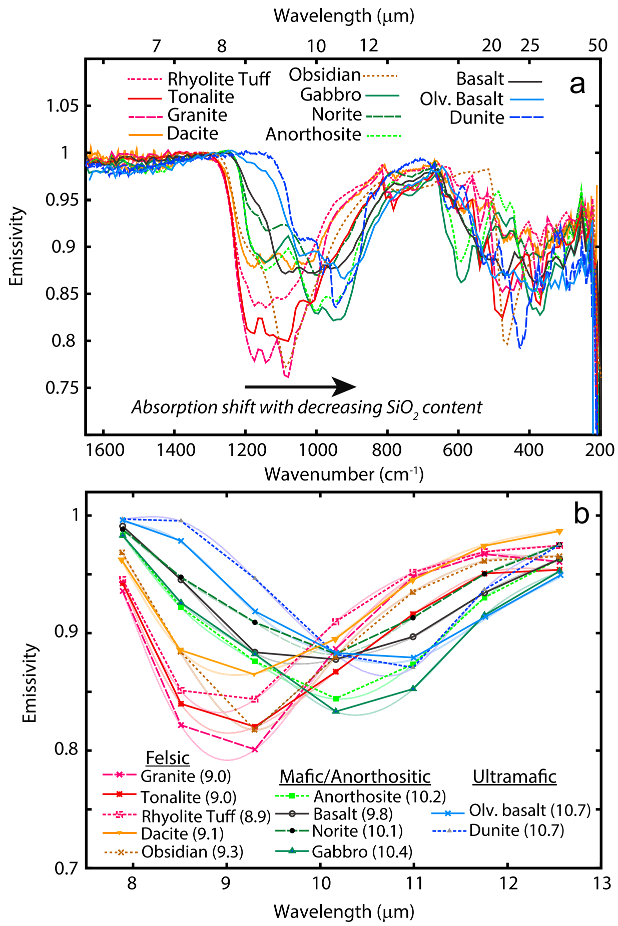

Figure 1. (a) Laboratory thermal emission spectra of felsic, anorthositic, mafic, and ultramafic rocks. These rocks are easily distinguished at laboratory spectral resolution (4 cm^{-1}). Note that the position of the collective Si-O absorption envelope between ~1250 and 800 cm^{-1} generally shifts to lower frequencies (higher wavelengths) with decreasing SiO_2 content [e.g., *Lyon*, 1965] (see also Figure S1). (b) Spectra from Figure 1a, degraded using the THEMIS filter response functions for bands 3–9. Thin faint curves are cubic spline fits to the THEMIS resolution spectra. Values in parentheses are the wavelength positions of the spline fit minima (SFM) in microns (see text for details). Felsic rocks are easily distinguished from anorthosite and mafic rocks. However, the loss of spectral detail complicates distinction of anorthosite from basalt.

values were calculated for a suite of volcanic rocks, ranging from basalts to dacites, analyzed by *Wyatt et al.* [2001] (Figure S1 in the supporting information). From Figures 1b and S1, it can be seen that felsic rocks exhibit SFM below ~9.3 μm. Note that the SFM position of pure obsidian glass ($SiO_2 \cong 75$ wt %) is ~9.3 μm, but felsic rocks with a crystalline component (quartz and feldspar) exhibit SFM < 9.2 μm. Anorthositic and mafic rocks exhibit SFM between ~9.7 and 10.4 μm, and ultramafic rocks exhibit SFM at wavelengths >10.6 μm.

Analyses of THEMIS multispectral images for five of the eight locations reported by *Carter and Poulet* [2013] and *Wray et al.* [2013] are shown in Figures 2 and S2. Locations for analysis were chosen based on areal extent and/or lack of reported colocated hydration detections, with the exception of Xanthe Terra. (Significant alteration could potentially obscure the THEMIS spectral character of the primary lithology.) Figure 2 shows that aside from dacitic lava flows in Nili Patera [*Christensen et al.*, 2005], none of the areas examined in Nili Patera or Noachis Terra exhibit THEMIS spectral characteristics that are consistent with felsic (or siliceous intermediate) rocks. For some of the areas where feldspar was detected with NIR data, THEMIS data are consistent with anorthositic, but not felsic lithologies. However, it is important to note that there are multiple lithologies with intermediate- to low-silica content (such as basalt) that are consistent with THEMIS data (Figure 1b). In Nili Patera, NIR feldspar detections are spectrally indistinguishable (in THEMIS data) from other high thermal inertia caldera floor materials, which have basaltic signatures. In Noachis Terra, the THEMIS spectral characteristics are also inconsistent with felsic rocks (Figure 2; see also *Rogers and Nazarian* [2013] for THEMIS spectra from additional Noachis locations). Though some locations exhibit SFM as low as ~9.4 μm, for these to be felsic would require a glass-dominant composition. This is not consistent with the NIR data or the THEMIS spectra (Figure 2). Rather, they most likely represent intermediate-silica compositions. In Holden crater, Tyrrhena Terra and Xanthe Terra, NIR-based feldspar detections are areally small in extent ($<$150,000 m^2) and exhibit low spectral contrast in THEMIS data, suggesting fine particle sizes that complicate determination of bulk composition in the TIR. Thus, evidence for felsic or anorthositic compositions is not present in THEMIS data over these regions (Figure S2); however, the small areal extent and/or small particle size likely prevent their detection (supporting information).

In Nili Patera and Noachis Terra, the thermal infrared data are not consistent with felsic interpretations. However, the geologic context of the Nili Patera and Noachis units suggests volcanic, rather than plutonic origins, also ruling out anorthositic lithologies for those two locations. This led us to consider alternative

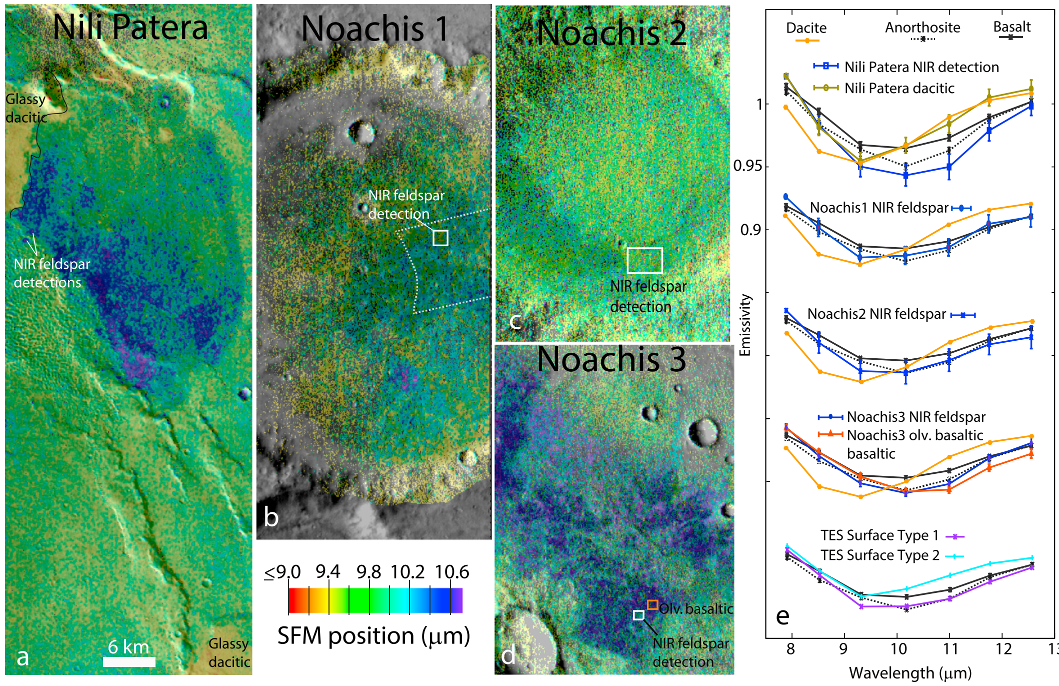

Figure 2. (a–d) Maps of THEMIS surface emissivity cubic spline fit minima (SFM) positions for reported feldspar-enriched regions in Nili Patera and Noachis Terra [*Wray et al*., 2013]. Using spectra from Figure 1b, felsic rocks should exhibit SFM $<\sim 9.3$ μm; anorthosites and basaltic materials exhibit SFM between 9.8 and 10.4 μm; ultramafic materials have SFM $>\sim 10.7$ μm. Areas with no color overlay exhibit low spectral emissivity depth (<0.03). Because low spectral depth is commonly associated with dust cover and/or nonlinear spectral mixing [e.g., *Rogers et al*., 2007], the SFM position cannot be related to bulk composition in the same manner as for coarse-grained surfaces. Hence, these pixels are masked out. (e) THEMIS spectra extracted from select regions coinciding with NIR feldspathic detections (rectangles in Figures 2b–2d) are shown. Nili Patera, THEMIS image I08561006 (Figure 2a). "NIR feldspar detections" indicates regions reported as felsic in *Wray et al*. [2013]. "Glassy dacitic" indicates surfaces reported as dacitic in *Christensen et al*. [2005] using TES and THEMIS data. THEMIS spectra from each of these units are shown in Figure 2e. Noachis Terra area 1 corresponds with area indicated by orange arrow in Figure 2 of *Wray et al*. [2013] (Figure 2b). THEMIS image I09611002. Much of the crater floor was suggested to be felsic from CRISM multispectral images [*Wray et al*., 2013]; the rectangle shows the location from which THEMIS spectra were extracted. Location of CRISM full resolution targeted image (FRT00008F08) in this area for reference. Noachis Terra area 2 corresponds with "area 1" from Figure 2 of *Wray et al*. [2013] (Figure 2c). THEMIS image I09948002. Rectangle shows the location from which THEMIS spectra were extracted. Noachis Terra area 3 corresponds with "area 4" from Figure 2 of *Wray et al*. [2013] (Figure 2d). White rectangle shows one of many NIR feldspar detections in this area, and the location of the THEMIS spectrum shown in Figure 2e. Orange rectangle shows the location of THEMIS spectra collected over the olivine basaltic unit reported in *Wray et al*. [2013] and *Rogers and Nazarian* [2013]. THEMIS image I08675002. THEMIS surface emissivity spectra from the areas indicated in Figures 2a–2d, compared with basalt, anorthosite, and dacite (Figure 2e). Dacite was conservatively chosen as the reference spectrum because it is at the border of intermediate and felsic rock compositions. Rhyolite and granite emissivity minima would be shifted to even shorter wavelengths (Figure 1). Global TES spectral end-members "Surface Types 1 and 2" [*Bandfield et al*., 2000] are also shown for comparison. The SFM positions for Surface Types 1 and 2 are 9.6 and 9.5 μm, respectively.

spectral analogs that would be consistent with constraints from the NIR, TIR, and geologic context of these units. Previous studies that determined the detection limit of plagioclase in NIR spectra of mineral mixtures used grain sizes <500 μm, for applicability to spectral measurements of lunar regoliths [*Nash and Conel*, 1974; *Crown and Pieters*, 1987; *Cheek et al*., 2013]. Figure 3 shows NIR spectra of coarse-grained (840–2000 μm) binary mixtures of augite and oligoclase. These data show that the broad, ~1.25 μm band due to plagioclase is detectable at lower abundances (at least as low as 50 vol %) compared to fine-grained mixtures. This is because larger grains are optically thick, reducing multiple photon interactions with the stronger-absorbing pyroxene grains. Thus, materials with relatively large plagioclase crystals, such as a plagioclase-megaphyric basalt, could be consistent with some of the weaker feldspathic detections identified from NIR data. For comparison, Figure 3 also shows the CRISM reflectance spectrum derived by *Rogers and Nazarian* [2013] for the light-toned units in Noachis Terra, as well as reflectance spectra from

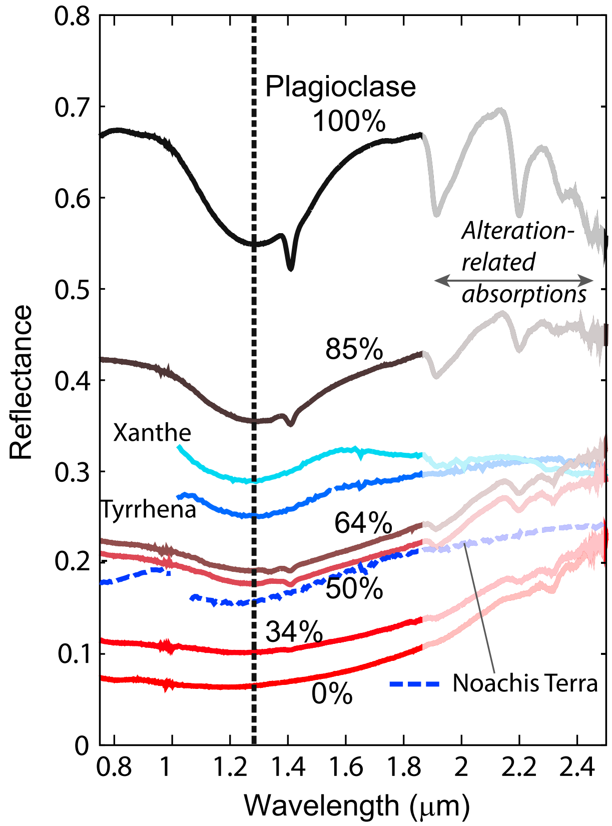

Figure 3. Near-infrared reflectance spectra of coarse-grained binary mixtures of oligoclase and augite. No offsets or scaling factors were applied. Augite grains are between 715 and 841 μm diameter and have the composition ($Ca_{1.0}Mg_{0.7}Fe_{Tot0.3}Si_2O_6$), confirmed by microprobe. Oligoclase grains are between 841 and 2000 μm and have the composition ($Ab_{75}An_{23}Or_2$), confirmed by microprobe. Coarse-grained plagioclase is detectable at abundances at least as low as 50 vol %. Note that the augite available to us had a very high Ca content; clinopyroxenes with very high Ca content commonly lack a ~2 μm band and also exhibit a broad asymmetrical ~1 μm band rather than a narrow and symmetrical band found in other clinopyroxenes [*Adams*, 1975; *Klima et al.*, 2011; *Horgan et al.*, 2014]. Plagioclase detection limits would likely differ with pyroxene composition of the matrix. Blue-toned spectra are CRISM-derived reflectance spectra from Noachis Terra, Tyrrhena Terra crater rim (64.7°E, 16.5°S), and Xanthe Terra (51.7°E, 2.7°N), shown for comparison. All three are ratios from the NIR feldspar detections to nearby spectrally featureless units and are offset by −0.8 (Noachis), −0.75 (Tyrrhena), and −0.65 (Xanthe). No scaling factors were applied. The "Noachis Terra" spectrum is from Figure 15 of *Rogers and Nazarian* [2013].

two other NIR detection locations in Xanthe Terra and Tyrrhena Terra. In the Noachis example, the depth of the ~1.2 μm feature is of the same magnitude of the 50/50 plagioclase-augite mixtures. For the other examples, the ~1.2 μm absorption is slightly deeper. Though we do not investigate plagioclase detectability for a wide variety of plausible coarse-grained mixtures here, these data demonstrate that abundances at least as low as 50% are detectable within a mafic matrix.

3. Possible Formation Mechanisms of Feldspar-Enriched Eruptive Products

In regions of thick continental crust on Earth, the bulk compositions of lavas from intraplate volcanoes appear largely controlled by fractionation of basalt at the base of the crust, while the mineralogy of the lavas reflects low-pressure crystallization after ascent of residual liquids formed at depth [e.g., *Nekvasil et al.*, 2000, 2004; *Whitaker et al.*, 2007, 2008]. This is shown schematically in Figure 4. As suggested by their study of "melt" inclusion assemblages of the Chassigny meteorite, *Nekvasil et al.* [2007, 2009] concluded that fractionation of rising mantle-derived magmas at the base of the crust should also be anticipated for Mars.

Fractionation at depth generally removes early-formed ferromagnesian minerals, thereby enriching the residual liquids in feldspar components. Table 1 provides an example of this for the Humphrey bulk composition [*Gellert et al.*, 2006] synthesized by *McCubbin et al.* [2008]. The normative feldspar content of the original Humphrey composition is 42 wt %. Using the residual liquid composition determined experimentally [*McCubbin et al.*, 2008] after 54% crystallization of the Humphrey composition (with 0.07 wt % dissolved water) at ~65 km depth, the normative feldspar content rises to 48 wt % in the residual liquid (Table 1, Residual Liquid A). Figure 4 and Table S1 show the computed mineral assemblages at low pressure (1 bar, QFM + 1) obtained using the MELTS thermodynamic model [*Ghiorso and Sack*, 1995] in order to compare the mineral assemblage formed from Humphrey composition liquid at the surface with that forming from Residual liquid A (if the latter separated from the minerals formed at the base of the crust, rose through the crust, and either ponded in a shallow magma chamber or erupted to form a thick, relatively slowly cooled, lava flow). Once 95% crystallinity was achieved for both Humphrey composition melt and Residual Liquid A at the surface, MELTS predicts that the unfractionated Humphrey basalt would contain 33% $An_{41}Ab_{58}Or_1$ andesine plagioclase, with the remainder of the rock

10.1002/2015GL063501

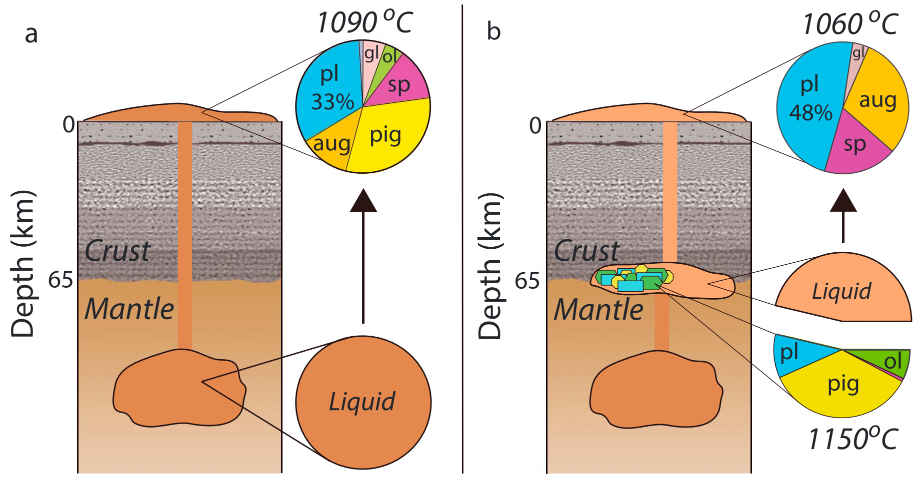

Figure 4. Schematic of mineralogy of lavas ~95% crystalline if a magma of Humphrey composition (0.07 wt % water) (a) ascended directly to the surface before crystallizing or (b) first underwent ~50 wt % crystallization at 65 km depth, and only residual liquids rose to the surface. For both cases, the final assemblages at low pressure were computed using the MELTS model [*Ghiorso and Sack*, 1995] for 1 bar (QFM + 1); the fractionating assemblage at depth in Figure 4b (plagioclase, pigeonite, and olivine) was determined experimentally by *McCubbin et al.* [2008]. Details of the computed low-pressure mineral assemblages are given in Table S1.

consisting of two pyroxenes, magnetite, and minor olivine (Table S1 and Figure 4a). In contrast, Residual Liquid A would produce 48% $An_{30}Ab_{67}Or_3$ calcic oligoclase plagioclase, with the remainder consisting of augite and magnetite (Table 1 and Figure 4b).

It is anticipated that the amount of plagioclase forming at 1 bar would be higher in residual liquids from a similar extent of high-pressure fractionation if the original Humphrey composition magma contained more dissolved water. Using the experimental liquid composition of *McCubbin et al.* [2008] after 51% crystallization of Humphrey-like liquids with 1.7 wt % water at 65 km depth, the amount of feldspar components in the norm of the residual liquid rises to 64% (Residual liquid B, Table 1), significantly higher than the 48% normative feldspar constituents of the “dry” residual melt. This increase in feldspar components in wet residual melts arises from the dissolution mechanism of water in silicate melt [*Burnham*, 1975; *Stolper*, 1982], which involves disrupting the bridging oxygens that link silica and alumina tetrahedra, depolymerizing the melt and decreasing the activities of the feldspar melt components. The lowered activities of the feldspar melt components suppress plagioclase stability temperatures [e.g., *Bohlen et al.*, 1982], thereby allowing a greater abundance of these components to build up in the melt before plagioclase crystallizes. Once the residual liquid rises and the water is lost to second boiling, the activities of the feldspar melt components increase again and the plagioclase crystallizes.

Given that both Nili Patera and Noachis Terra are associated with thick highlands crust, the production of feldspar-rich lavas can be expected and remains a reasonable explanation, self-consistent with the observations and context. Though viscosity depends on a number of factors, the associated silica contents for the residual liquids are low and their Fe contents remain elevated (Table 1) [*McCubbin et al.*, 2008], which would favor the capacity to deposit such lavas across broad areal extents. Thus, the feldspar-enriched nature of the Noachis Terra light-toned units does not preclude an effusive origin.

Table 1. Variation in Feldspar Abundance in Humphrey and Derivative Melts

Liquid Compositions	SiO_2 (wt %)	TiO_2	Al_2O_3	FeO	MgO	CaO	Na_2O	K_2O	P_2O_5	Normative Feldspar
Synthetic Humphrey	48.6	0.5	11.1	18.2	9.7	8.2	2.8	0.2	0.6	42
Residual liquid A[a]	47.4	0.9	13.5	18.5	5.0	9.0	4.1	0.3	1.2	48
Residual liquid B[b]	51.2	0.7	16.3	14.6	3.2	8.0	4.7	0.3	1.1	64

[a]A Residual liquid after 54% crystallization, 9.3 kbar, 0.07 wt % water (1150°C).
[b]B Residual liquid after 51% crystallization, 9.3 kbar, 1.67 wt % water (1030°C).

4. Conclusions

Thermal infrared data do not support felsic interpretations for the NIR-based feldspathic rock detections in Nili Patera and Noachis Terra reported by *Wray et al*. [2013]. Anorthositic compositions, which are spectrally similar to basalts at THEMIS spectral resolution, are permitted by the thermal infrared data in some areas, however. This is an important distinction, as felsic rocks imply high-silica contents and typically require either extensive low-pressure fractionation or significant amounts of crustal recycling/incorporation to form.

If plagioclase crystals are large ($>$~840 μm), they can be detected in mineral mixtures with mafics at abundances at least as low as 50 vol % (Figure 3). This value is much lower than the previously stated requirement of $<$15% mafics for detection, which was based on finer grain sizes typical of regoliths [e.g., *Crown and Pieters*, 1987]. Thus, anorthositic or felsic interpretations need not be invoked for all NIR-based feldspar detections. In particular, areally large units in Nili Patera and Noachis Terra are unlikely to be plutonic in origin, ruling out anorthositic interpretations for those two locations. Rather, a plagioclase-megaphyric basaltic unit would be most consistent with the NIR, TIR, and geologic context observations in those regions. Plagioclase-phyric basalts have been observed at Gale crater with the Mars Science Laboratory Curiosity Rover [*Sautter et al*., 2014] and are the dominant texture found in the Martian meteorite NWA 7034 (a basaltic breccia) [*Agee et al*., 2013; *Santos et al*., 2015]. In addition, possible pyroclastic rocks with large plagioclase crystals were identified at Gusev crater with the Spirit rover ("Wishstone" class rocks) [*Ruff et al*., 2006]. Thus, plagioclase-phyric basalts may be more than a rare occurrence in Martian highlands materials.

Plagioclase-enriched basaltic eruptive products can be formed from known Martian basaltic compositions ("Humphrey") investigated by the Spirit rover through partial crystallization at the base of a thick crust, followed by low-pressure crystallization of the residual liquids. Consistent with emerging discoveries of evolved rock types at Gusev crater [*Ruff et al*., 2006; *Squyres et al*., 2006], Gale crater [*Sautter et al*., 2014], and within NWA 7034 [*Santos et al*., 2015], the combined interpretation of NIR and TIR data over Nili Patera and Noachis Terra suggest magmatic fractionation processes took place throughout Martian history, in a variety of highland locations on Mars.

Acknowledgments
We thank Steve Ruff (ASU), Don Lindsley, and the Stony Brook University planetary discussion group for useful conversations on this topic. A.D.R. acknowledges funding from the Mars Odyssey project and NASA Mars Data Analysis Program NNX14AM26G. Both authors acknowledge funding from the NASA Mars Fundamental Research Program NNX13AG82G. We appreciate constructive comments from Francis McCubbin and an anonymous reviewer. All Mars data shown in this manuscript are available from the Planetary Data System. JMARS software was used to locate, assemble, and analyze the various image data sets. We thank Vicky Hamilton for providing the thermal emission spectra presented in *Wyatt et al*. [2001].

The Editor thanks two anonymous reviewers for their assistance in evaluating this paper.

References

Adams, J. B. (1975), Interpretation of visible and near-infrared diffuse reflectance spectra of pyroxenes and other rock-forming minerals, in *Infrared and Raman Spectroscopy of Lunar and Terrestrial Minerals*, edited by C. Karr, pp. 91–116, Academic Press, New York.

Adams, J. B., and L. H. Goullaud (1978), Plagioclase feldspars: Visible and near infrared diffuse reflectance spectra as applied to remote sensing, *Proc. Lunar Planet. Sci. Conf.*, *9*, 2901–2909.

Agee, C. B., et al. (2013), Unique meteorite from early Amazonian Mars: Water-rich basaltic breccia Northwest Africa 7034, *Science*, *339*, 780–786.

Bandfield, J. L., V. E. Hamilton, and P. R. Christensen (2000), A global view of Martian surface compositions from MGS-TES, *Science*, *287*(5458), 1626–1630.

Bandfield, J. L., D. Rogers, M. D. Smith, and P. R. Christensen (2004), Atmospheric correction and surface spectral unit mapping using Thermal Emission Imaging System data, *J. Geophys. Res.*, *109*(E10), E10008, doi:10.1029/2004JE002289.

Bohlen, S. R., A. L. Boettcher, and V. J. Wall (1982), The system Ab-H_2O-CO_2: A model for melting and activities of water at high pressures, *Am. Mineral.*, *67*, 451–462.

Burnham, C. W. (1975), Water and magmas: A mixing model, *Geochim. Cosmochim. Acta*, *39*, 1077–1084.

Carmichael, I. S. E. (1964), The petrology of Thingmuli, a Tertiary volcano in eastern Iceland, *J. Petrol.*, *5*, 435–460.

Carter, J., and F. Poulet (2013), Ancient plutonic processes on Mars inferred from the detection of possible anorthositic terrains, *Nat. Geosci.*, *6*, 1008–1012, doi:10.1038/ngeo1995.

Chappell, B. W., A. J. R. White, I. S. Williams, and D. Wyborn (2004), Low- and high-temperature granites, *Geol. Soc. Am. Spec. Pap.*, *389*, 125–140.

Cheek, L. C., K. L. Donaldson Hanna, C. M. Pieters, J. W. Head, and J. L. Whitten (2013), The distribution and purity of anorthosite across the Orientale basin: New perspectives from Moon Mineralogy Mapper data, *J. Geophys. Res. Planets*, *118*, 1805–1820, doi:10.1002/jgre.20126.

Christensen, P. R., et al. (2004), The Thermal Emission Imaging System (THEMIS) for the Mars 2001 Odyssey Mission, *Space Sci. Rev.*, *110*(1–2), 85–130.

Christensen, P. R., et al. (2005), Evidence for magmatic evolution and diversity on Mars from infrared observations, *Nature*, *436*, 504–509.

Crown, D. A., and C. M. Pieters (1987), Spectral properties of plagioclase and pyroxene mixtures and the interpretation of lunar soil spectra, *Icarus*, *72*, 492–506.

Emslie, R. F. (1978), Anorthosite massifs, rapakivi granites, and late Proterozoic rifting of North America, *Precamb. Res.*, *7*, 61–98.

Gellert, R., et al. (2006), Alpha particle X-ray spectrometer (APXS): Results from Gusev crater and calibration report, *J. Geophys. Res.*, *111*, E02S05, doi:10.1029/2005JE002555.

Ghiorso, M. S., and R. O. Sack (1995), Chemical mass-transfer in magmatic processes 4: A revised and internally consistent thermodynamic model for the interpolation and extrapolation of liquid–solid equilibria in magmatic systems at elevated-temperatures and pressures, *Contrib. Mineral. Petrol.*, *119*(2–3), 197–212.

Hook, S. J., J. E. Dmochowski, K. A. Howard, L. C. Rowan, K. E. Karlstrom, and J. M. Stock (2005), Mapping variations in weight percent silica measured from multispectral thermal infrared imagery—Examples from the Hiller Mountains, Nevada, USA and Tres Virgenes-La Reforma, Baja California Sur, Mexico, *Remote Sens. Environ.*, *95*, 273–289, doi:10.1016/j.rse.2004.11.020.

Horgan, B. H. N., E. A. Cloutis, P. Mann, and J. F. Bell (2014), Near-infrared spectra of ferrous mineral mixtures and methods for their identification in planetary surface spectra, *Icarus*, *234*, 132–154, doi:10.1016/j.icarus.2014.02.031.

Klima, R. L., M. D. Dyar, and C. M. Pieters (2011), Near-infrared spectra of clinopyroxenes: Effects of calcium content and crystal structure, *Meteorit. Planet. Sci.*, *46*, 379–395, doi:10.1111/j.1945-5100.2010.01158.

Le Maitre, R. W. (1976), The chemical variability of some common igneous rocks, *J. Petrol.*, *17*, 589–637.

Lindsley, D. H., B. R. Frost, C. D. Frost, and J. S. Scoates (2010), Petrology, geochemistry and structure of the Chugwater Anorthosite, Laramie Anorthosite Complex, Southeastern Wyoming, *Can. Min.*, *48*, 887–923.

Longhi, J. (2003), A new view of lunar ferroan anorthosites: Postmagma ocean petrogenesis, *J. Geophys. Res.*, *108*(E8), 5083, doi:10.1029/2002JE001941.

Lyon, R. J. P. (1965), Analysis of rocks by spectral infrared emission (8 to 25 microns), *Econ. Geol.*, *60*, 715–736.

McCubbin, F. M., H. Nekvasil, A. D. Harrington, S. M. Elardo, and D. H. Lindsley (2008), Compositional diversity and stratification of the Martian crust: Inferences from crystallization experiments on the picrobasalt Humphrey from Gusev Crater, Mars, *J. Geophys. Res.*, *113*, E11013, doi:10.1029/2008JE003165.

Nash, D. B., and J. E. Conel (1974), Spectral reflectance systematics for mixtures of powdered hypersthene, labradorite, and ilmenite, *J. Geophys. Res.*, *79*(11), 1615–1621.

Nekvasil, H., A. Simon, and D. H. Lindsley (2000), Crystal fractionation and the evolution of intra-plate hy-normative igneous suites: Insights from their feldspars, *J. Petrol.*, *41*, 1743–1757.

Nekvasil, H., A. Dondolini, J. Horn, J. Filiberto, H. Long, and D. H. Lindsley (2004), The origin and evolution of silica-saturated alkalic suites: An experimental study, *J. Petrol.*, *45*(4), 693–721.

Nekvasil, H., J. Filiberto, F. M. McCubbin, and D. H. Lindsley (2007), Alkalic parental magmas for the chassignites?, *Meteorit. Planet. Sci.*, *42*, 979–992.

Nekvasil, H., F. M. McCubbin, A. Harrington, S. Elardo, and D. H. Lindsley (2009), Linking the Chassigny meteorite and the Martian surface rock Backstay: Insights into igneous crustal differentiation processes on Mars, *Meteoritics Planet. Sci.*, *44*, 853–869.

Pan, C., A. D. Rogers, and J. R. Michalski (2015), Thermal and near-infrared analyses of central peaks of Martian impact craters: Evidence for a heterogeneous Martian crust, *J. Geophys. Res. Planets*, *120*, doi:10.1002/2014JE004676, in press.

Rogers, A. D., and A. H. Nazarian (2013), Evidence for Noachian flood volcanism in Noachis Terra, Mars, and the possible role of Hellas impact basin tectonics, *J. Geophys. Res. Planets*, *118*, 1094–1113, doi:10.1002/jgre.20083.

Rogers, A. D., J. L. Bandfield, and P. R. Christensen (2007), Global spectral classification of Martian low-albedo regions with Mars Global Surveyor Thermal Emission Spectrometer (MGS-TES) data, *J. Geophys. Res.*, *112*, E02004, doi:10.1029/2006JE002726.

Rogers, A. D., O. Aharonson, and J. L. Bandfield (2009), Geologic context of in situ rocky exposures in Mare Serpentis, Mars: Implications for crust and regolith evolution in the cratered highlands, *Icarus*, *200*, 446–462, doi:10.1016/j.icarus.2008.11.026.

Ruff, S. W., P. R. Christensen, D. L. Blaney, W. H. Farrand, J. R. Johnson, J. R. Michalski, J. E. Moersch, S. P. Wright, and S. W. Squyres (2006), The rocks of Gusev Crater as viewed by the Mini-TES instrument, *J. Geophys. Res.*, *111*, E12S18, doi:10.1029/2006JE002747.

Santos, A. R., C. B. Agee, F. M. McCubbin, C. K. Shearer Jr., P. V. Burger, R. Tartèse, and M. Anand (2015), Petrology of igneous clasts in Northwest Africa 7034: Implications for the petrologic diversity of the Martian crust, *Geochim. Cosmochim. Acta*, *157*, 56–85, doi:10.1016/j.gca.2015.02.023.

Sautter, V., et al. (2014), Igneous mineralogy at Bradbury Rise: The first ChemCam campaign at Gale crater, *J. Geophys. Res. Planets*, *119*, 30–46, doi:10.1002/2013JE004472.

Skok, J. R., J. F. Mustard, B. L. Ehlmann, R. E. Milliken, and S. L. Murchie (2010), Silica deposits in the Nili Patera caldera on the Syrtis Major volcanic complex on Mars, *Nat. Geosci.*, *3*, 838–841, doi:10.1038/ngeo990.

Smith, M. R., J. L. Bandfield, E. A. Cloutis, and M. S. Rice (2013), Hydrated silica on Mars: Combined analysis with near-infrared and thermal-infrared spectroscopy, *Icarus*, *223*, 633–648, doi:10.1016/j.icarus.2013.01.024.

Squyres, S. W., et al. (2006), Rocks of the Columbia Hills, *J. Geophys. Res.*, *111*, E02S11, doi:10.1029/2005JE002562.

Stolper, E. (1982), The speciation of water in silicate melts: An infrared spectroscopic study, *Geochim. Cosmochim. Acta*, *46*, 2609–2620.

Ueberhuber, C. W. (1997), *Numerical Computation 1*, pp. 353–438, Springer, Berlin.

Whitaker, M. L., H. Nekvasil, D. H. Lindsley, and N. J. Difrancesco (2007), The role of pressure in producing compositional diversity in intraplate basaltic magmas, *J. Petrol.*, *48*, 365–393.

Whitaker, M. L., H. Nekvasil, D. H. Lindsley, and M. McCurry (2008), Can crystallization of olivine tholeiite give rise to potassic rhyolites? An experimental investigation, *Bull. Volcanol.*, *70*, 417–434.

Wray, J. J., S. T. Hansen, J. Dufek, G. A. Swayze, S. L. Murchie, F. P. Seelos, J. R. Skok, R. P. Irwin, and M. S. Ghiorso (2013), Prolonged magmatic activity on Mars inferred from the detection of felsic rocks, *Nat. Geosci.*, *6*, 1013–1017, doi:10.1038/ngeo1994.

Wyatt, M. B., V. E. Hamilton, H. Y. McSween, P. R. Christensen, and L. A. Taylor (2001), Analysis of terrestrial and Martian volcanic compositions using thermal emission spectroscopy: 1. Determination of mineralogy, chemistry, and classification strategies, *J. Geophys. Res.*, *106*(E7), 14711, doi:10.1029/2000JE001356.